Evaluation of the exactness of the approximate quantum numbers A and T of doubly excited helium states

Bao Cheng-guang
Chinese Center of Advanced Science and Technology (World Laboratory), P.O. Box 8730, Beijing 100 080, China and Department of Physics, Zhongshan University, Guangzhou, China

Duan Yiwu
Department of Physics, Xiangtan Normal College, Xiangtan, Hunan Province, China
(Received 17 January 1992)

The approximate quantum numbers A and T in the $(K,T)^A$ classification scheme of doubly excited helium states have been evaluated. A strong mixing of the symmetrized and antisymmetrized components has been found in the $A=0$ states. A direct verification supporting rotorlike structures has also been found.

PACS number(s): 31.50.+w, 31.20.Tz, 31.20.Di, 31.90.+s

I. INTRODUCTION

It is well known that the ${}_n(K,T)^A_N$ scheme [1,2] is successful in classifying doubly excited helliumlike states. In this notation, N (n) labels the shell where the inner (outer) electron stays; K is an integer to describe the angular separation between the two electrons: A ($=+$, $-$, or 0) describes the symmetry with interchanging r_1 and r_2 (r_i is the norm of $\mathbf{r}_i$ originating from the nucleus); $T=|m'|$, m' is the projection of the total orbital angular momentum $\mathbf{L}$ along the direction of $\mathbf{r}_1-\mathbf{r}_2$. Recently, a new set of quantum numbers $n_\lambda n_\mu m$ based on the molecular-orbital description was proposed [3,4], where n_λ, n_μ, and m are quantum numbers associated with the prolate spheroidal coordinates λ, μ, and φ. It was shown in [3] that in certain states the motion associated with the variation of λ is independent from that of μ.

These two schemes can be considered essentially equivalent in the sense that the set of quantum numbers of one scheme can be reproduced by those of the other scheme by the following relations:

$$\begin{aligned} &A=(-1)^{n_\mu},\quad \tfrac{1}{2}(N-K-T-1)=n_\lambda\ , \\ &T=|m|,\quad K=\{n_\mu-[1-(-1)^{n_\mu}]/2\}/2-n_\lambda\ . \end{aligned} \tag{1}$$

However, the $A=0$ states in the $(K,T)^A$ scheme have no counterpart in the $(n_\lambda n_\mu m)$ scheme. Both schemes are approximate schemes in the sense that both sets of quantum numbers are approximate quantum numbers. It is the aim of this paper to determine the exactness of these numbers by extracting relevant information directly from numerical solutions of the exact Hamiltonian. These solutions are obtained via a procedure outlined in [5], which is essentially a variational procedure; the solutions obtained are not very accurate (the accuracy is roughly the same as those by Lipsky, Anania, and Conneely [6]). However, since we are concerned mainly with the qualitative aspect, they are accurate enough for qualitative purposes.

Let us denote an (anti)symmetrized partial-wave (PW) channel by

$$(l_1l_2)^{\pm}=\epsilon_{\pm}\{[Y_{l_1}(\hat{\mathbf{r}}_1)Y_{l_2}(\hat{\mathbf{r}}_2)]_L\pm[Y_{l_1}(\hat{\mathbf{r}}_2)Y_{l_2}(\hat{\mathbf{r}}_1)]_L\}\ , \tag{2}$$

where $l_2\geq l_1$, and $\epsilon_{\pm}=1/\sqrt{2}$ ($l_1\neq l_2$) or $[1\pm(-1)^L]/4$ ($l_1=l_2$). Evidently, $(l_1l_2)^+$ is symmetric with interchanging $\hat{\mathbf{r}}_1$ and $\hat{\mathbf{r}}_2$, while $(l_1l_2)^-$ is antisymmetric.

Let the spatial part of the eigenwave functions be expanded as

$$\Psi=\sum_{l_1\leq l_2}\left[\frac{G^{(a)}_{l_1l_2}(r_1r_2)}{r_1r_2}(l_1l_2)^+ + \frac{G^{(b)}_{l_1l_2}(r_1r_2)}{r_1r_2}(l_1l_2)^-\right]\ . \tag{3}$$

Let us define

$$W^a=\sum_{l_1\leq l_2}\int dr_1dr_2|G^{(a)}_{l_1l_2}|^2 \tag{4}$$

and

$$W^b=\sum_{l_1\leq l_2}\int dr_1dr_2|G^{(b)}_{l_1l_2}|^2\ . \tag{5}$$

Let W^+ (W^-) be the weight of the symmetric (antisymmetric) component of Ψ with respect to the interchange of r_1 and r_2 fulfilling $W^++W^-=1$. Evidently, in the case of total spin $S=0$. We have $W^+=W^a$, and $W^-=W^b$; in $S=1$, the reverse is true. The deviation of W^+ from 1 or 0 measures the exactness of the quantum number A. Let us further define

$$W_{l_1l_2}=\int dr_1dr_2(|G^{(a)}_{l_1l_2}|^2+|G^{(b)}_{l_1l_2}|^2)\ . \tag{6}$$

This is the weight of a PW channel, i.e., the weight of

having one electron (either the inner or the outer one) in l_1 and the other one in l_2. These quantities show the PW composition of a state. In what follows, the ${}^3P^e$, ${}^1P^o$, ${}^1D^o$, ${}^3D^e$ states with $N=3$, $n \leq 5$ are examined.

II. EIGENENERGIES AND THE PARTIAL-WAVE COMPOSITION

The results are given in Table I. The first column gives the $(K,T)^A$ and $(n_\lambda n_\mu m)$ labels, and the second column gives n. Then, in each L,S,π state, the energy and the $W_{l_1 l_2}$ are given from left to right; the energy calculated by Lipsky [6] is also given in parentheses for a comparison.

This table shows several things:

(i) Among the states having the same L,S,π, those having the same $(K,T)^A$ have similar PW composition. The qualitative feature of this composition does not change with n; however, increasing n usually results in stronger mixing of the PW components.

(ii) Among the states having the same ${}_n(K,T)^A_N$, states having different L,S,π have different PW compositions. However, we shall see that the difference affects mainly the collective rotation but not the internal motion, as shown later.

III. EVALUATION OF THE A NUMBER

The exactness of A is shown by W^+ given in Table II (since $W^+ + W^- = 1$, only giving W^+ is sufficient). This table shows that the mixing of the symmetric and antisymmetric components is, in general, remarkable. There are some noticeable points:

(i) Evidently, there are three types of states: the first type (having $A=+1$) has a much larger W^+, and the second (having $A=-1$) has a much larger W^-, while the third (having $A=0$) has very strong mixing of the symmetric and antisymmetric components. It appears as that there is no explicit border (or gap) to separate the W^+ (or W^-) into three regions. The existence of the states with particularly strong mixing implies the definite existence of the $A=0$ states; however, they have no counterpart in the $(n_\lambda n_\mu m)$ scheme.

(ii) In order to understand the details of mixing, let us first rewrite the Hamiltonian as

$$H = H_{\text{con}} + H_{\text{mix}} , \tag{7}$$

where

$$H_{\text{con}} = -\frac{1}{2}\left(\frac{1}{r_1^2}\frac{\partial}{\partial r_1} r_1^2 \frac{\partial}{\partial r_1} + \frac{1}{r_2^2}\frac{\partial}{\partial r_2} r_2^2 \frac{\partial}{\partial r_2}\right) + \tfrac{1}{4}(\ell_1^2+\ell_2^2)\left(\frac{1}{r_1^2}+\frac{1}{r_2^2}\right) - \frac{z}{r_1} - \frac{z}{r_2} + \frac{1}{r_{12}} \tag{8}$$

keeps the symmetry with interchanging r_1 and r_2, where ℓ_i is the operator of the orbital angular momentum of the ith electron;

$$H_{\text{mix}} = \tfrac{1}{4}(\ell_1^2 - \ell_2^2)\left(\frac{1}{r_1^2} - \frac{1}{r_2^2}\right) \tag{9}$$

TABLE I. The eigenenergies E_i (in eV) and the weights of the partial-wave channel $W_{l_1 l_2}$ of the ${}^3P^e$, ${}^1P^o$, ${}^1D^o$, and ${}^3D^e$ states having $N=3$ and $n \leq 5$. Values in parentheses are from a calculation by Lipsky [6].

		${}^3P^e$				${}^1P^o$				${}^1D^o$				${}^3D^e$				
$(K,T)^A$ $(n_\lambda n_\mu m)$	n	E_i	W_{11}	W_{22}	W_{33}	E_i	W_{01}	W_{12}	W_{23}	E_i	W_{12}	W_{23}	E_i	W_{02}	W_{11}	W_{13}	W_{22}	W_{24}
$(1,1)^+$	3	−9.160(−9.169)	0.81	0.19		−9.068(−9.124)	0.53	0.46	0.01	−8.923(−8.955)	0.98	0.02	−8.842(−8.881)	0.94	0.01	0.05		
(021)	4	−7.390(−7.398)	0.72	0.28		−7.367(−7.376)	0.44	0.50	0.06	−7.297(−7.314)	0.95	0.05	−7.271(−7.284)	0.86	0.01	0.12		0.01
	5	−6.832(−6.835)	0.67	0.33		−6.815(−6.823)	0.40	0.55	0.05	−6.784(−6.784)	0.87	0.13	−6.769(−6.778)	0.83	0.01	0.08	0.07	0.01
$(-1,1)^+$	3	−7.909(−7.918)	0.22	0.75	0.03	−7.665(−7.683)	0.40	0.39	0.21									
(101)	4	−6.898(−6.903)	0.33	0.66	0.01	−6.843(−6.851)	0.44	0.29	0.27									
$(2,0)^-$	4					−7.818(−7.788)	0.80	0.19	0.01				−7.699(−7.708)	0.42	0.51	0.03	0.04	
(050)	5					−7.006(−7.011)	0.74	0.25	0.01				−6.963(−6.970)	0.42	0.48	0.05	0.05	
$(0,0)^-$	4					−7.286(−7.288)	0.21	0.63	0.16				−7.113(−7.124)	0.11	0.24	0.31	0.30	0.04
(130)	5					−6.754(−6.761)	0.26	0.56	0.18				−6.680(−6.690)	0.13	0.24	0.30	0.26	0.07
$(0,2)^-$	4									−7.333(−7.344)	0.84	0.16	−7.338(−7.345)	0.27	0.09	0.06	0.57	0.01
(012)	5									−6.775(−6.795)	0.84	0.16	−6.778(−6.786)	0.19	0.07	0.14	0.56	0.04
$(-2,0)^0$	4					−6.677(−6.689)	0.16	0.35	0.49									
$(-1,1)^0$	4									−6.860(−6.883)	0.26	0.74	−6.818(−6.831)	0.36	0.19	0.21	0.05	0.19
	5									−6.571(−6.592)	0.31	0.69						

TABLE II. The weights of the symmetrized components of states having $N=3$.

$(K,T)^A$ $(n_\lambda n_\mu m)$	n	$^3P^e$	$^1P^o$	$^1D^o$	$^3D^e$
$(1,1)^+$	3	1	0.91	0.83	0.76
(021)	4	1	0.88	0.86	0.77
	5	1	0.89	0.77	0.69
$(-1,1)^+$	3	1	0.85		
(101)	4	1	0.76		
$(2,0)^-$	4		0.07		0.12
(050)	5		0.06		0.12
$(0,0)^-$	4		0.22		0.25
(130)	5		0.20		0.28
$(0,2)^-$	4			0.22	0.11
(012)	5			0.31	0.17
$(-2,0)^0$	4		0.61		
$(-1,1)^0$	4			0.52	0.37
	5			0.46	0.32

mixes up the symmetric and antisymmetric components. Evidently, the extent of the mixing is determined by the matrix elements of H_{mix}.

Now, in the $^3P^e$ states, since $l_1=l_2$ as shown in Table I, there is no mixing. In the $^1P^o$ states, there are mainly the (01), (12), and (23) PW components having $|l_1(l_1+1)-l_2(l_2+1)|$ equal to 2, 4, and 6, respectively. We found that the $(2,0)^-$ states are dominated by the (01) component, as shown in Table I, and thus they have a smaller mixing. On the other hand, the main component in the $(-2,0)^0$ states is the (23) component, and thus it results in a larger mixing. This explains the background of the numbers in Table II. Since the states having different K have different PW structures, thus the extent of mixing depends on K.

Another example is the $^3D^e$ states. Where the $(1,1)^+$ states are dominated by the (02) component resulting in stronger mixing; the largest components in the $(2,0)^-$ and $(0,2)^-$ states are (11) and (22), respectively, resulting in weaker mixing.

Now let us compare the mixing in a rotor series having the same ${}_n(K,T)_N^A$ but different L,S,π. An example is the ${}_n(1,1)_3^+$ states, where the $^3P^e$ states are dominated by the (11) component, the $^1P^o$ states by a mixture of the (01) and (12) components, the $^1D^o$ states by the (12) component, and finally the $^3D^e$ states by the (02) component. Thus in this series $|\langle \ell_1^2-\ell_2^2\rangle|$ gets increasingly larger. Consequently, the mixing also gets increasingly larger. Thus the exactness of A in different states of a rotor series is different; it depends on the PW structures.

(iii) The factor $(1/r_1^2-1/r_2^2)$ is not as important as the difference in orbital angular momenta. When N and n both become large (both electrons are far away from the nucleus), the mixing is, in general, weaker. When N is fixed and n is increasing, this factor is, in general, larger; however, the effect from increasing n is weak.

IV. EVALUATION OF THE T NUMBER

An evaluation of the T number has been recently made in Ref. [7] by numerical calculation to obtain the weight of each T component. In this paper, we use another procedure to make the evaluation. The advantage of the present procedure is that the angular correlation of the electrons can be evaluated at the same time, and the main structure of the wave function can also be revealed, as follows.

Let us define a body frame with its k' axis parallel to $\mathbf{r}_1-\mathbf{r}_2$. Then Ψ can be expanded as

$$\Psi=\sum_{m'=-L}^{L} D^L_{m'M}(\mathcal{R})\frac{Q_{m'}(r_1r_2\theta_{12})}{r_1r_2}\ , \tag{10}$$

where θ_{12} is the angle between $\mathbf{r}_1$ and $\mathbf{r}_2$, $\mathcal{R}$ denotes the Euler angles, m' is the projection of L along the k' axis, and $T=|m'|$. From the symmetries with respect to the interchange of $\mathbf{r}_1$ and $\mathbf{r}_2$, and to the reflection, we have

$$Q_{m'}(r_1r_2\theta_{12})=\pi(-1)^{m'+L}Q_{\bar{m}'}(r_1r_2\theta_{12})\ , \tag{11}$$

$$Q_{m'}(r_1r_2\theta_{12})=\pi(-)^{m'+S}Q_{m'}(r_2r_1\theta_{12})\ . \tag{12}$$

Inserting Eq. (11) into Eq. (10), we have

$$\Psi=\sum_{m'=0}^{L}\tilde{D}^L_{m'M}\tilde{Q}_{m'}/r_1r_2\ , \tag{13}$$

$$\tilde{D}^L_{m'M}=D^L_{m'M}+\pi(-)^{m'+L}D^L_{\bar{m}'M}\ , \tag{14}$$

where $\tilde{Q}_{m'}=Q_{m'}$ $(m'\neq 0)$, and $\tilde{Q}_0=Q_0/2$. Evidently, the factor $\tilde{D}^L_{m'M}$ describes the collective rotation, while $\tilde{Q}_{m'}$ describes the internal motion. If in Eq. (13) only one m' component is dominant, as we shall show, the coupling between these two kinds of motion is weak.

Now let us define a pair of distances r_{in} and r_{out} for each state. r_{in} (r_{out}) is the most probable distance that e_{in} (e_{out}) prefers to stay. These pairs of distances can be obtained from the one-body densities defined later (also refer to [5]). In what follows we shall present the results on $\tilde{Q}_{m'}$ by a number of figures, where $\tilde{Q}_{m'}$ are considered as functions of θ_{12} with r_1 given at r_{in} and r_2 given at r_{out}.

Figures 1(a)–1(d) show the $^3P^e$, $^1P^o$, $^1D^o$, and $^3D^e$ states of the ${}_4(1,1)_3^+$ supermultiplet, respectively. We found that the internal structures of these four states are essentially the same, and are all dominated by the $m'=1$ component; the shapes of the curves $\tilde{Q}_1$ are very similar, in particular, the peak of each curve is closer to the right, which implies a larger angular separation in a positive-K state. This finding is a direct verification of the rotorlike structure. However, this description is not exact. Only in the $^3P^e$ state is the $m'=1$ component pure; there is a small amount of the $m'=0$ component mixed in the $^1P^o$ state, the $m'=2$ component mixed in the $^1D^o$ state, and both the $m'=0$ and 2 components mixed in the $^3D^e$ state.

Although these states have similar internal structures, they have different ways of collective rotation. This arises because the $\tilde{D}^L_{m'M}(\mathcal{R})$ factor is π and L dependent. Accordingly, the system may prefer different orientations in these different states. This situation is shown by the

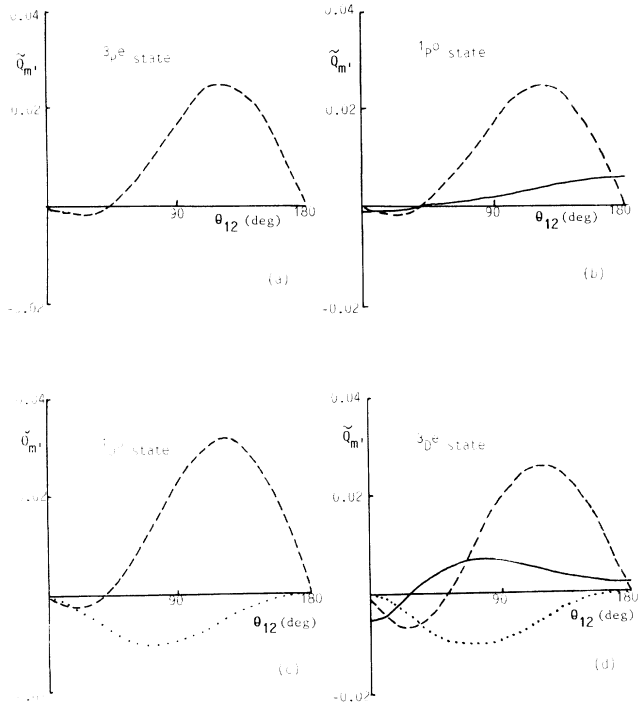

FIG. 1. $\tilde{Q}_{m'}$ of the ${}_4(1,1)_3^+$ supermultiplet as functions of θ_{12} when r_1 is given at r_{in} and r_2 at r_{out}. The solid line is for $m'=0$, the dashed line is for $m'=1$, and the dotted line is for $m'=2$.

one-body densities defined as

$$\rho_1(r_1\theta_1)=4\pi r_1^2\int d\mathbf{r}_2|\Psi|^2\ , \tag{15}$$

where θ_1 is the angle between $\mathbf{r}_1$ and the Z axis. Figures 2(a)–2(d) show ρ_1 of the above four states as a function of

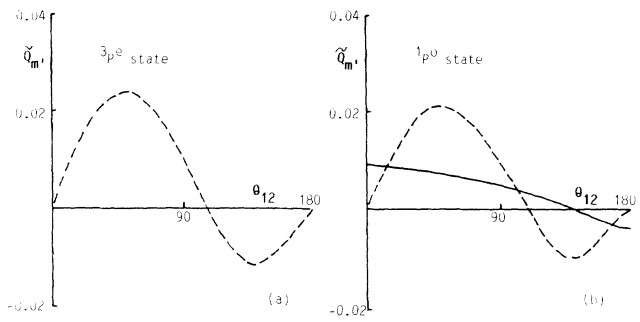

FIG. 3. $\tilde{Q}_{m'}$ of the ${}_4(-1,1)_3^+$ supermultiplet (refer to Fig. 1).

r_1 when θ_1 is specified. In these figures, we have M (the projection of L on the Z axis) equal to $|\mathbf{L}|$, such that $\mathbf{L}$ is essentially lying along the Z axis. Thus, the anisotropism of the distribution shown in these figures is relative to the direction of $\mathbf{L}$. Different members of the supermultiplet do exhibit different anisotropism. In particular, the electrons strongly prefer lying along $\mathbf{L}$ in the $^3P^e$ state, but prefer lying in the plane perpendicular to $\mathbf{L}$ in the $^3D^e$ state. Incidentally, the location of the main peak of ρ_1 (in the $N=3$ shell) is defined as r_{in}, and that of the outmost peak is defined as r_{out} in each state. If we change n from 4 to 5, we find that the above qualitative features of the ${}_4(1,1)_3^+$ supermultiplet remain unchanged.

Figures 3(a) and 3(b) show the $\tilde{Q}_{m'}$ of the ${}_4(-1,1)_3^+$ supermultiplet. Here we recover the similarity of the internal structures. It is also dominated by the $m'=1$ component. The $m'=0$ component intrudes in the $^1P^o$ state as before; however, now the $\tilde{Q}_1$ lies closer to the left, which implies a smaller angular separation in the

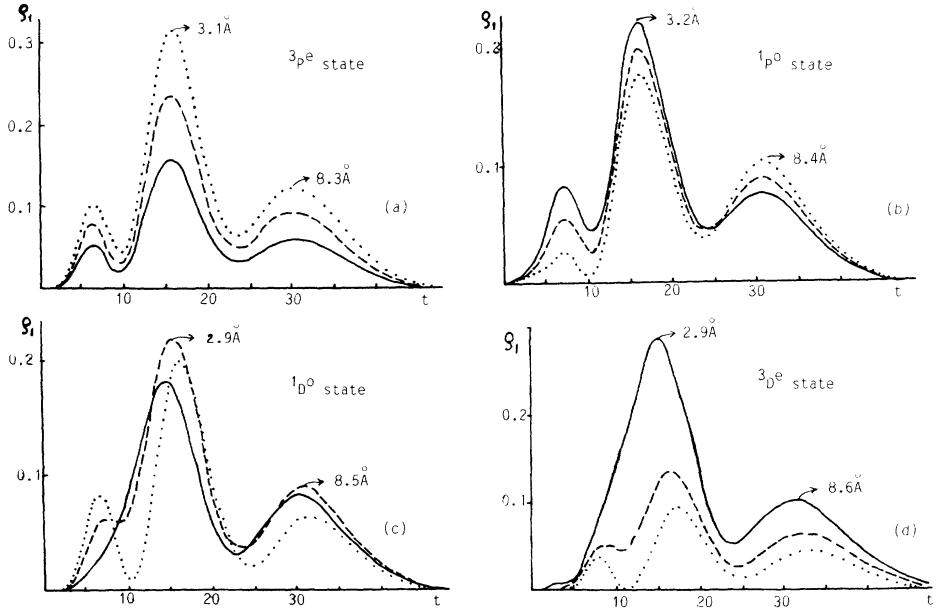

FIG. 2. One-body densities ρ_1 of the ${}_4(1,1)_3^+$ supermultiplet. ρ_1 is plotted as a function of r_1 when θ_1 is given at 90° (solid line), 45° (dashed line), and 0° (solid line), respectively. The abscissa t is related to r by $r=0.05t^{1.5}$ Å. In each state the z component of $\mathbf{L}$ is equal to L.

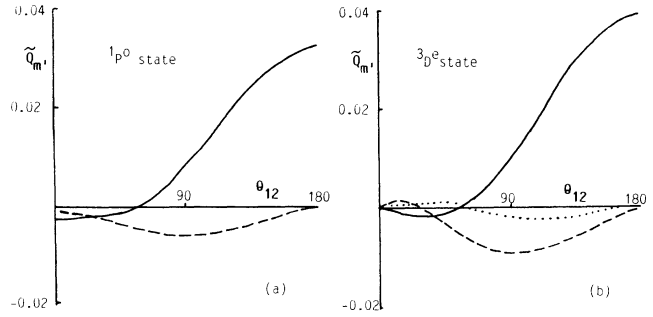

FIG. 4. $\tilde{Q}_{m'}$ of the ${}_4(2,0)_3^-$ supermultiplet (refer to Fig. 1).

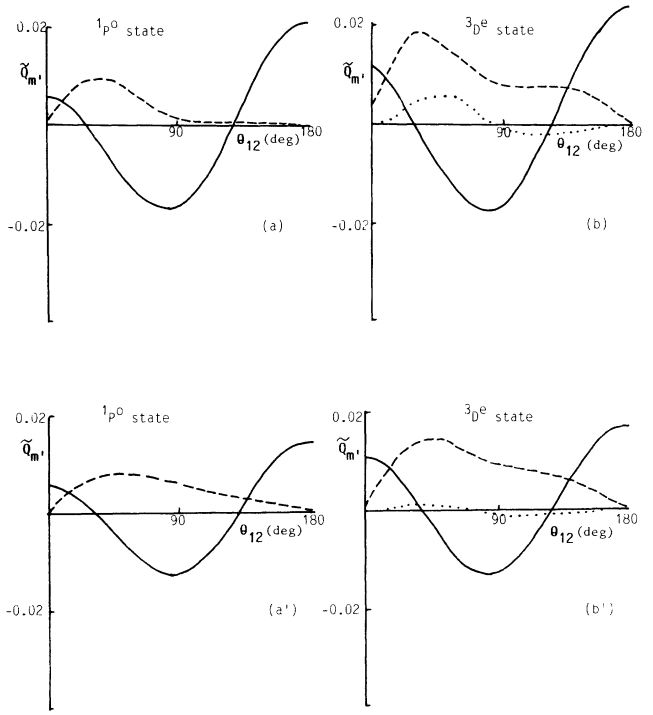

FIG. 5. (a) and (b) $\tilde{Q}_{m'}$ of the ${}_4(0,0)_3^-$ supermultiplet (refer to Fig. 1). (a') and (b') are the same as (a) and (b) but with $n=5$.

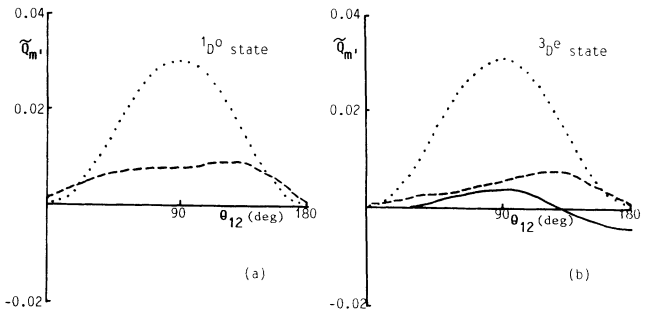

FIG. 6. $\tilde{Q}_{m'}$ of the ${}_4(0,2)_3^-$ supermultiplet (refer to Fig. 1).

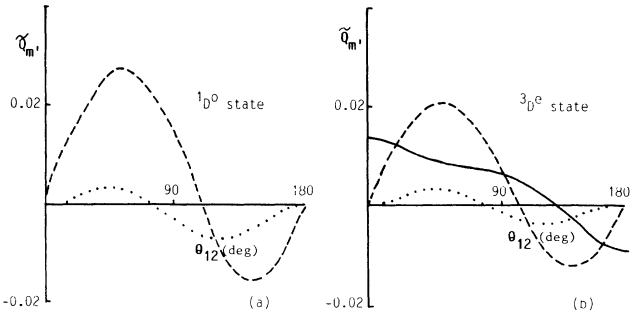

FIG. 7. $\tilde{Q}_{m'}$ of the ${}_4(-1,1)_3^0$ supermultiplet (refer to Fig. 1).

negative-K states.

Figures 4(a) and 4(b) are for the ${}_4(2,0)_3^-$ supermultiplet. These two figures are very similar; besides, the $^3D^e$ state contains a small amount of the $m'=2$ component. Figures 5(a) and 5(b) are for the ${}_4(0,0)_3^-$ supermultiplet; when $n=4$ changes to $n=5$, Figs. 5(a) and 5(b) change to Figs. 5(a') and 5(b'), respectively. We found several things:

(i) The main component has $m'=0$ with two nodes, and there is a great distribution around $\theta_{12}=90°$. This suggests the quantum numbers $T=0$ and $K=0$.

(ii) The $^3D^e$ states have a stronger T mixing than the $^1P^o$ states. It is expected that larger L will result in stronger mixing.

(iii) The $n=5$ states do not, in general, have a stronger mixing than the $n=4$ states.

Figures 6(a) and 6(b) are for the ${}_4(0.2)_3^-$ supermultiplet, where the $^1D^o$ state cannot have the $m'=0$ component due to Eq. (11). Evidently, the wave functions are dominated by $m'=2$ component and are mainly distributed around the $\theta_{12}=90°$ region. The similarity in internal structures inside this supermultiplet is once more explicit.

Figures 7(a) and 7(b) are for the ${}_4(-1.1)_3^0$ supermultiplet, where the distributions shifts to the left. Figure 8 is for the ${}_4(-2,0)_3^0$ supermultiplet. This figure can be compared with Fig. 4(a) to show the great difference in angular correlation. It is noticeable that this state has $A=0$, and has very strong A mixing, as shown in Table I. However, it does not have particularly strong T mixing.

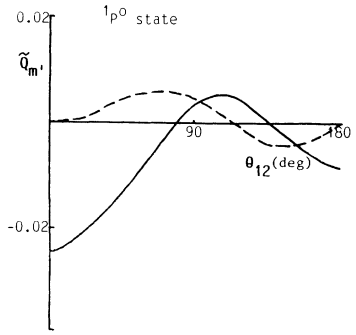

FIG. 8. $\tilde{Q}_{m'}$ of the ${}_4(-2,0)_3^0$ supermultiplet (refer to Fig. 1).

V. FINAL REMARKS

It is emphasized that the emphasis of this paper has been only in the qualitative aspect. Though the wave functions under consideration are not very accurate, the following facts related to the accuracy are noticeable:

(i) The basis functions used in this paper are well chosen. As stated, the set of single-electron basis functions

$$\rho_k(r)=\mathcal{N}_k e^{-\gamma r/2} r^{l+1} L_n^{2l+2}(\gamma r) \tag{16}$$

has been used successfully in [8]; where the extent of the distribution is determined by the adjustable parameter γ, all basis functions have the same γ. In our model space, we use similar but improved basis functions, where γ may not be the same for all basis functions. Since, in fact, the extent of the distribution of an electron depends strongly on the effective charge arising from the nucleus and from the screening effect of the other electron, in our procedure the γ of each basis function is strictly related to the effective charge, which is adjustable in an interval depending on the status of the other electron. With the defrozen γ, our model space become purer and more effective in the sense that it is less contaminated by the spurious components from the continuum. As a result, most eigenstates are stable with respect to the change in dimension and in parameters. For example, in the $N=3$ series of the ${}^3D^e$ states, the eigenenergies obtained by us in a smaller (64-dimensional) and in a larger (134-dimensional) model space are listed in Table III, where the stability is explicit. The energies by Lipsky, Anania, and Conneely (shown in Table I) are, in general, lower than ours; this may arise because the $2lnl'$ basis functions are excluded in their $N=3$ calculations.

(ii) We have used an additional judgment to evaluate the accuracy of the solutions by calculating

$$\varepsilon_i=\langle\Psi_i|\mathcal{T}+E_i|\Psi_i\rangle/E_i\ , \tag{17}$$

where $\mathcal{T}$ is the total kinetic-energy operator. According to the virial theorem, ε_i should be zero if Ψ_i is exact; hence, if $|\varepsilon_i|$ is large, Ψ_i must be far apart from the exact solution (the reverse is not necessarily true). It turns out that once our model space is suitably chosen, the eigenstates can be explicitly divided into two groups; one has very small $|\varepsilon_i|$, while the other has very large $|\varepsilon_i|$. This is shown in Table IV, where the ε_i of the eigenstates adjacent to the lowest ${}^3D^e$ state of the $N=3$ series are given. This table shows that a few states have exceptionally large $|\varepsilon_i|$; this implies that the spurious components are heavily concentrated in these states, and they should be eliminated. After the elimination, the rest of the model space is expected not to be seriously contaminated by spurious components.

(iii) Although Table III shows a small change in energies when the dimension of the model space is enlarged, we found that the qualitative features of the wave functions remain unchanged. For example, let us observe the weights of the partial-wave channels $W_{l_1 l_2}$ of the ${}^3D^e$ states [defined in Eq. (6) and shown in Table I]. We found that most of them have only a 0.01–0.02 change when the model space is enlarged from 64 dimensions to 134 dimensions. Accordingly, the related figures of $\bar{Q}_{m'}$ change only very slightly.

(iv) Although primarily the results of the $N=3$, $n=4$ states have been presented, many other states of the $N=3$ series and states of the $N=2$ series have also been investigated. Thus, what we provide is a systematic knowledge of the spectrum and not only the information of a particular state.

Since we have used a reasonable model space, since most spurious components can be eliminated, since the qualitative features of the wave functions remain unchanged when we enlarge the model space, and since the qualitative features are extracted from systematic observations, we conclude that, though we have not yet obtained very accurate solutions in the quantitative sense, the information extracted is reliable in the qualitative sense. We found several things:

(i) The mixing of the symmetric and antisymmetric components is remarkable. Since the mixing is contributed mainly by the factor $\langle \ell_1^2-\ell_2^2\rangle$, the details of mixing

TABLE III. The eigenenergies E_i (in eV) of the $N=3$ series of the ${}^3D^e$ states obtained in a 64-dimensional space (column one) and in a 134-dimensional space (column two).

${}^3D^e$	
64 dimensions	134 dimensions
−8.842	−8.847
−7.699	−7.697
−7.338	−7.336
−7.271	−7.271
−7.113	−7.112
−6.963	−6.964
−6.817	−6.820
−6.778	−6.777
−6.769	−6.770
−6.680	−6.679

TABLE IV. ε_i [refer to Eq. (17)] of a sequence of adjacent ${}^3D^e$ states close to the head state of the $N=3$ series. These states are obtained via a diagonalization of the Hamiltonian in a 64-dimensional space.

${}^3D^e$	
E_i (eV)	ε_i
−13.750	−0.227
−13.335	−0.297
−9.331	−1.834
−8.842	−0.004
−7.699	−0.003
−7.338	−0.001
−7.271	−0.005
−7.113	−0.002
−6.963	+0.001
−6.817	0
−6.778	−0.002
−6.769	−0.002

are explicitly PW dependent. The mixing can be quantitatively measured by W^+ (or W^-), and may be close to 1, 0, or $\frac{1}{2}$; thus not only the positive- and negative-A states, but also the $A=0$ states are necessary to classify roughly the symmetry of the states. It is noticeable that the $A=0$ states have no counterpart in the molecular-orbital model [3], and thus the correspondence between the $(K,T)^A$ scheme and the $(n_\lambda n_\mu m)$ scheme should be carefully checked.

(ii) The exact definition of the collective rotation and the internal motion depends on the choice of the body frame. If the body frame is chosen with its k' axis parallel to $\mathbf{r}_1-\mathbf{r}_2$, then we find from the states under investigation that the coupling between the collective and internal motions is, in general, weak. Accordingly, the mixing of the m' components is weak, and the T number is approximately conserved. In fact, direct verification has been found to support the rotorlike structures; namely, the states belonging to the same supermultiplet have similar internal structures. The mixing is also PW dependent. For example, Figs. 5(a) and 5(b) show that the $^3D^e$ state has a much stronger mixing than the $^1P^o$ state. In fact, it has already been found in [7] that the extent of mixing will increase when L increases.

(iii) In the states under investigation, the $(K,T)^A$ scheme works in general. However, we do see that some states have W^+ to be close to $\frac{3}{4}$ or $\frac{1}{4}$, and in some states the mixing of different m' components is very strong (e.g., those in Figs. 5(b), 5(b'), and 7(b); in these states, A and T are far from exact quantum numbers. Nonetheless, they are still valuable numbers to expose some of the underlying physics.

[1] D. R. Herrick and O. Sinanoglu, Phys. Rev. A **11**, 97 (1975).
[2] C. D. Lin, Adv. At. Mol. Phys. **22**, 77 (1986).
[3] J. M. Feagin and J. S. Briggs, Phys. Rev. Lett. **57**, 984 (1986); Phys. Rev. A **37**, 4599 (1988).
[4] J. M. Rost, R. Gersbacher, K. Richter, J. S. Briggs, and D. Wintgen, J. Phys. B **24**, 2455 (1991).
[5] C. G. Bao, Phys. Rev. A **38**, 591 (1988).
[6] L. Lipsky, R. Anania, and M. J. Conneely, At. Data Nucl. Tables **20**, 127 (1977).
[7] Z. Chen, C. G. Bao, and C. D. Lin, J. Phys. B **25**, 61 (1992).
[8] R. Gersbacher and J. T. Broad, J. Phys. B **23**, 365 (1990).